Acta Pharmaceutica Sinica B 2020;10(4):680–692

Chinese Pharmaceutical Association
Institute of Materia Medica, Chinese Academy of Medical Sciences

Acta Pharmaceutica Sinica B

www.elsevier.com/locate/apsb
www.sciencedirect.com

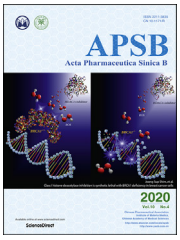

ORIGINAL ARTICLE

Effect of fluid shear stress on the internalization of kidney-targeted delivery systems in renal tubular epithelial cells

Yingying Xu[†], **Shuo Qin**[†], **Yining Niu, Tao Gong, Zhirong Zhang, Yao Fu**[*]

Key Laboratory of Drug-Targeting and Drug Delivery Systems of Ministry of Education and Sichuan Province, Sichuan Engineering Laboratory for Plant-Sourced Drug and Sichuan Research Center for Precision Industrial Technology, West China School of Pharmacy, Sichuan University, Chengdu 610041, China

Received 4 June 2019; received in revised form 12 September 2019; accepted 31 October 2019

KEY WORDS

Fluid shear stress;
Kidney-targeted drug delivery;
HK-2 cells;
Acute kidney injury

Abstract Renal tubular epithelial cells (RTECs) are important target cells for the development of kidney-targeted drug delivery systems. Under physiological conditions, RTECs are under constant fluid shear stress (FSS) from original urine in the renal tubule and respond to changes of FSS by altering their morphology and receptor expression patterns, which may affect reabsorption and cellular uptake. Using a microfluidic system, controlled shear stress was applied to proximal tubule epithelial cell line HK-2. Next, 2-glucosamine, bovine serum albumin, and albumin nanoparticles were selected as representative carriers to perform cell uptake studies in HK-2 cells using the microfluidic platform system with controlled FSS. FSS is proven to impact the morphology of HK-2 cells and upregulate the levels of megalin and clathrin, which then led to enhanced cellular uptake efficiencies of energy-driven carrier systems such as macromolecular and albumin nanoparticles in HK-2 cells. To further investigate the effects of FSS on endocytic behavior mediated by related receptors, a mice model of acute kidney injury with reduced fluid shear stress was established. Consistent with *in vitro* findings, *in vivo* studies have also shown reduced fluid shear stress down-regulated the levels of megalin receptors, thereby reducing the renal distribution of albumin nanoparticles.

*Corresponding author. Tel.: +86 28 85503798.
E-mail address: yfu4@scu.edu.cn (Yao Fu).
[†]These authors made equal contributions to this work.

Peer review under the responsibility of Chinese Pharmaceutical Association and Institute of Materia Medica, Chinese Academy of Medical Sciences.

https://doi.org/10.1016/j.apsb.2019.11.012

1. Introduction

As a vital organ maintaining the homeostasis of human body, kidney plays critical roles in regulating acid-base balance, electrolyte concentration, extracellular fluid volume and blood pressure[1]. The nephron, including the renal corpuscle (the glomerulus and Bowman's capsule) and the tubules (proximal convoluted tubules, loop of Henle, and distal tubules), constitutes the structural and functional unit of kidney[2]. Urine formation in the nephron takes two steps: glomerulus filtration and renal tubule reabsorption. Epithelial cells at the proximal convoluted tubules display high metabolic activity for reabsorption of water, small molecules, peptides, and proteins[2]. The sodium−hydrogen exchange, and megalin−cubilin mediated endocytosis in proximal tubule epithelial cells have shown to respond to changes of fluid shear stress (FSS) in the renal tubules[3,4]. In the past few decades, studies have demonstrated that mechanical forces such as FSS extensively impact cellular and tissue morphology, and their functions as well[5]. For example, physical forces impact cytoskeletal organization, gene expression, proliferation, survival, and the internalization of therapeutic nanoparticles in different manners[6,7].

Renal disorders often include acute injury and chronic kidney diseases (CKD). Acute kidney injury may result in dysfunctions including reduced glomerular filtration, hypertension, urinary tract infections, and inflammation-related diseases[8−10]. CKD may lead to permanent renal damages through persistent loss of kidney function and during the terminal phase of CKD, and patients have to rely on repeated dialysis or even renal transplantation to maintain their kidney function[8,11]. To date, effective yet safe treatment options remain limited for patients with various renal disorders. This is partially due to the difficulty of drug delivery to kidney *via* systemic administration. To achieve a sufficient therapeutic concentration in the kidney often requires a higher dose to increase drug distribution at the disease site. However, when using higher doses, the lack of drug distribution specificity may result in systemic toxicity[12]. Moreover, even though drugs can be distributed to the kidney *via* dosage upregulation, they may not be efficiently delivered to the target cells under certain pathological conditions such as abnormal glomerular filtration[13].

To tackle problems mentioned above, kidney-targeted delivery system has been proposed to increase the efficacy and reduce the toxicity of therapeutics for treatment of various kidney diseases[12]. Specifically, the use of small molecule ligands[14], macromolecular carriers[15] and nanoparticles are common strategies used to achieve renal specific drug delivery[12]. Transporters located in the renal proximal tubules play important roles in tubular secretion and reabsorption of molecules in the kidney[16]. Megalin receptors, for example, are highly expressed in the proximal tubule epithelium of the kidney, which are selected as a target to develop kidney-targeted delivery systems[14]. A small molecule ligand, 2-glucosamine (GLN), is proven an effective ligand that can specifically bind to the megalin receptors and mediate internalization of prodrugs or drug conjugates into proximal tubule epithelial cells[14]. Serum albumin is another carrier for renal targeted drug delivery, which can be freely-filtrated by glomerulus and reabsorbed *via* megalin-mediated internalization in proximal tubules[4]. As previously reported, albumin exhibited high binding capacity for small molecule drugs, and excellent biocompatibility, which made it an ideal candidate for drug delivery[17,18]. Despite the extensive works on kidney-targeted delivery systems, most of them were performed under static conditions and failed to take into account the effect of FSS on renal tubular epithelial cells. Here, our study aimed to establish an *in vitro* platform system to investigate the impact of FSS on the uptake behavior of various kidney-targeted drug delivery systems in renal tubular epithelial cells by applying a stable and continuous FSS to cells[19]. To achieve this goal, a microfluidic system was established to provide better control over the environment for culturing cells under flow conditions. Cell morphology and selected receptors under both static and flow conditions were then characterized and compared accordingly. Next, fluorescein isothiocyanate (FITC)-labeled 2-GLN, FITC-labeled bovine serum albumin (BSA), and albumin nanoparticles were selected as model carriers to explore their internalization behaviors in HK-2 under both culturing conditions. Moreover, an *in vivo* study was performed to compare the distribution profiles of albumin nanoparticles under normal and disease state.

2. Materials and methods

2.1. Chemicals and reagents

Glucosamine hydrochloride was purchased from Kelong Chemical Reagent Factory (Chengdu, China). FITC, coumarin 6 (C6), and BSA were obtained from Sigma−Aldrich (Shanghai, China). Dimethyl sulfoxide (DMSO, analytical grade) was purchased from Kemiou (Tianjin, China). All the other chemicals and reagents were of analytical grade and obtained commercially.

2.2. Animals

BALB/c mice (male; body weight: 22 ± 2 g) were provided by Dashuo Biotechnology (Chengdu, China) and maintained in a germ-free environment with free access to food and water. All animal experiments were approved by the Institutional Animal Care and Ethics Committee of Sichuan University (approved No. SYXK2013-113).

2.3. Cell culture and microfluidic platform setup

An immortalized proximal tubule epithelial cell line, HK-2, was obtained from Shanghai Institute of Cell Biology (CAS, Shanghai, China). HK-2 cells were cultured in Dulbecco's modified Eagle's medium (DMEM) with high glucose (GIBCO, Carlsbad, CA, USA) and supplemented with 10% bovine serum (Fumeng, Shanghai, China), 100 IU/mL penicillin and 100 μg/mL streptomycin. Cells were maintained in a humidified incubator containing 5% CO_2 at 37 °C.

The ibidi μ-slide I 0.4 luer (ibidi, Martin Reid, Germany) with a volume of 100 μL was selected as the flow chamber for the following studies. The slides were pre-incubated at 37 °C with 5% CO_2 for 24 h prior to the seeding of cells to avoid air bubbles inside the channels. Then, HK-2 cells were carefully seeded into the μ-slide channel at a concentration of 1.2×10^6 cells/mL in 100 μL of cell suspension from one side of the channel. To avoid air bubbles, pipet tip was directly placed into the channel's inlet and applied the volume with a constant and swift flow. After cell attachment, 60 μL of culture medium was then filled in each

channel. The entire μ-slide was placed in a 10 cm Petri dish with wet sterile cotton to keep the environment moisturized. Culture medium was replaced every day.

The microfluidic control system consisted of a tubing with an inner-diameter of 1.5 mm and adapters (ibidi) for the connection between the ibidi μ-slide I 0.4 luer and HL-1S constant flow pump (Qingpu Huxi, Shanghai, China) (Fig. 1). HK-2 cells were seeded as mentioned above and cultured under the following flow condition for 2.5 h at 37 °C. Fluid shear stress was calculated using Eqs. (1)−(3) [20]:

$$\tau = \eta \cdot 131.6 \cdot \Phi \quad (1)$$

$$\tau = 0.2\ \text{dyne}/\text{cm}^2,\ \eta = 1.4\ \text{dyne}\cdot\text{s}/\text{cm}^2 \quad (2)$$

$$\Phi = 0.1\ \text{mL}/\text{min} \quad (3)$$

where τ is shear stress (dyne/cm^2), η is dynamical viscosity (dyne·s/cm^2) and Φ represents flow rate (mL/min).

2.4. Synthesis and characterization

2.4.1. FITC-GLN conjugation

Glucosamine hydrochloride in the amount of 220 mg were dissolved in 2 mL of water, and then mixed with 20 mg of FITC that was dissolved in 3.64 mL of DMSO and left to stand at 30 °C for three days[21]. The reactants were supplemented with 10-fold of deionized water, and then freeze-dried. The lyophilized product was dispersed in deionized water and then centrifuged at 2000×g (RJ-TDL-40B centrifuge, RUIJIANG instrument, Wuxi, China) for 10 min to remove the excessive amount of 2-GLN. FITC-GLN conjugate was precipitated as a yellow solid, which was then freeze-dried to obtain the dry product (yield, 67%). The ^{1}H NMR analysis was performed with an AMX-400 Bruker Spectrometer (Bruker, Beijing, China; Supporting Information Fig. S1) to confirm the conjugation.

2.4.2. FITC-BSA conjugation

A 40-mg of BSA was dissolved in 2 mL of carbonate buffer solution (CBS, pH 9.6). FITC was also dissolved in CBS to a final concentration of 1 mg/mL. Then, FITC solution was slowly added to the BSA solution at a feed ratio of 4:1 and the reaction was carried out at 4 °C for 12 h. The reactant solution was poured into a dialysis bag (molecular weight cut-off 3500) and dialyzed against deionized water for 48 h. After dialysis, FITC-BSA solution was then freeze-dried, and stored at 4 °C. The number of FITC molecules conjugated in FITC−BSA was determined by detecting the quantity difference of free amino residue in BSA and FITC-BSA after conjugation. Briefly, 40.71 mg of *o*-phthalaldehyde (OPA) was dissolved in 1 mL of methanol, and 3.81 g of sodium tetraborate was dissolved in water, and diluted to 100 mL to obtain a solution with concentration of 0.1 mol/L. Then, the solution was mixed with 20% sodium dodecyl sulfate (SDS) solution and 100 μL β-mercaptoethanol, and diluted with water to a final volume of 50 mL to obtain OPA reaction solution. L-Leucine standard solutions in different concentrations (200 μL each), 0.75 mg/mL of BSA, and FITC-BSA were reacted with 4 mL of OPA reaction solution for 5 min, respectively. According to the standard curve (Supporting Information Fig. S2) and intensity values, the free amino residuals of BSA solution was determined as equal to 0.027 mg/mL L-leucine solution and the value of FITC-BSA solution equal to 0.0053 mg/mL L-leucine. Thus, the ratio of free amino residues in BSA and FITC-BSA is 5:1, indicating that there are 46 FITC molecules per each FITC-BSA conjugate.

2.4.3. C6-BSA nanoparticle preparation

C6 was dissolved in a mixture of methylene chloride and ethyl acetate (7:3, *v*/*v*) to a final concentration of 100 μg/mL. A 10-mL of 2% BSA solution was mixed with 15, 20, and 25 mg of soybean oil, respectively. Next, 1 mL of C6 solution was added, and ultrasonicated using a probe sonicator for 8 min at 200 W, followed by rotary evaporation to remove the organic solvent[22]. The mean particle size, polydispersity index (PDI) and zeta potential of BSA-NPs were determined by dynamic light scattering analyzer (Zetasizer Nano ZS90, Malvern, Shanghai, China) (Supporting Information Table S1 and Fig. S3).

2.4.4. FITC-BSA nanoparticle preparation

A 2-mL of mixed solvent (dichloromethane:ethyl acetate = 7:3) was added with 25.4 mg of soybean oil as the oil phase, 200 mg of BSA and 100 mg of FITC-BSA dissolved in 10 mL of deionized water as the aqueous phase, and the two phases were mixed. After that, it was sonicated in an ice bath (power 330 W, 8 min), and then evaporated to remove organic solvent. The mean particle size, PDI and zeta potential of BSA-NPs were determined by dynamic light scattering analyzer (Zetasizer Nano ZS90; Supporting Information Table S2 and Fig. S4).

2.5. Cell uptake study

HK-2 cells were seeded in 12-well culture plates (NEST, Wuxi, China) at a seeding density of 2 × 10^5/cm^2. FITC-BSA was diluted into serum-free DMEM medium at final concentrations of 5, 50, and 500 μg/mL, respectively, and added to the HK-2 cells for 2 h incubation at 37 °C (n = 3). At the end of the uptake, cells were washed three times with phosphate buffer solution (PBS) to remove excessive liquid. Cells were then incubated with 200 μL of trypan blue for 3 min to quench the membrane-bound fluorescence[23] and washed with PBS 3 times. Afterwards, cells were digested with 0.2% trypsin and resuspended in 500 μL of PBS after centrifugation and discarding of supernatant. Cellular uptake efficiency was determined by FACScan Aria™ flow cytometry (Becton Dickison, Franklin Lake, NJ, USA).

HK-2 cells were cultured as described above. FITC and FITC-GLN were diluted into serum-free DMEM medium at a final concentration of 0.84 mmol/L[14]. FITC-BSA was diluted into serum-free DMEM medium at a final concentration of 50 μg/mL. BSA-NPs with sizes of 100, 150, and 200 nm were diluted into DMEM medium at a final concentration of 25 μg/mL[24]. Cells were then exposed to FITC, FITC-GLN, FITC-BSA, or BSA-NPs, respectively, and incubated for 5, 30, 60, and 120 min each. Trypan blue solution (50 μL, 0.4% *w*/*v*, Invitrogen, Carlsbad, CA, USA) was then added to the cells to quench the membrane-bound fluorescence probes. Cellular uptake efficiency was determined by flow cytometry.

To evaluate the effect of temperature on cell uptake rate, HK-2 cells were cultured as described above and then exposed to FITC, FITC-GLN, FITC-BSA, or BSA-NPs, and incubated for 2 h at 37 and 4 °C, respectively, following similar procedure described above.

To elucidate the impact of megalin receptors, cells were pre-incubated in 1 mL of 2 mg/mL of free glucosamine for 10 min before exposure to FITC and FITC-GLN as previously described[14]. Cells were then incubated with 0.84 mmol/L FITC or FITC-GLN for 2 h,

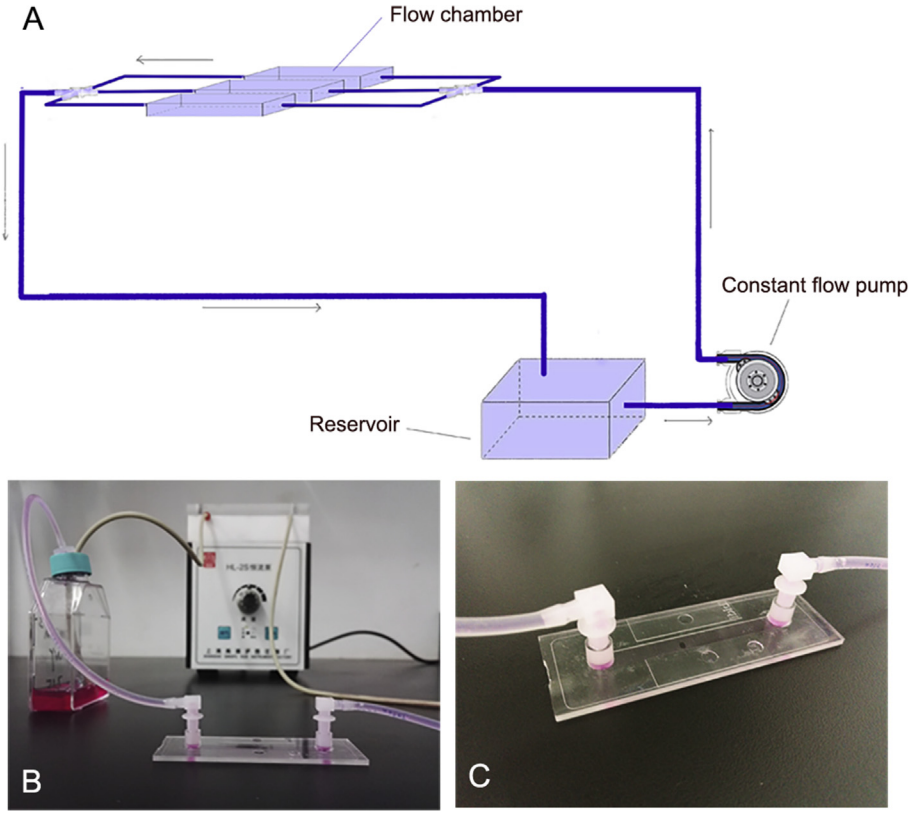

Figure 1 The microfluidic control system consists of a constant flow pump, a flow chamber and a reservoir. (A) The schematic diagram of the microfluidic system setup; (B) photo of the microfluidic system; and (C) the ibidi μ-slide I 0.4 luer.

and cellular uptake efficiency was determined by flow cytometry and compared with cells without the addition of inhibitor after quenching the membrane-bound fluorescence with trypan blue. In comparison, HK-2 cells were also pre-incubated with megalin antibody (rabbit polyclonal IgG, Abcam, dilution 1:250), 1 mmol/L ethylenediaminetetraacetic acid (EDTA), and 4 mg/mL gentamycin for 60 min, respectively, before the uptake study. Cells were then exposed to 50 μg/mL of FITC-BSA for 2 h at 37 °C. Cell uptake efficiency was determined by flow cytometry.

C6-BSA-NPs, with a size of 100 nm, were diluted in DMEM at a final concentration of 25 μg/mL. Cells were incubated with 0.5 mL of chlorpromazine (Clo, 30 mmol/L), sodium azide (NaN_3, 15.4 mmol/L), methyl-β-cyclodextrin (M-β-CD, 10 mmol/L), dimethyl amiloride (DMA, 100 mmol/L) and nystatin (Nys, 25 mmol/L) for 2 h, respectively. Then cells were exposed to BSA-NPs for 1 h at 37 °C. Cellular uptake efficiency was determined by flow cytometry in comparison with cells without the addition of inhibitors.

2.6. *Comparison of cell uptake in flow and static conditions*

HK-2 cells were seeded in the ibidi μ-slide I 0.4 luer, with 100 μL of 1.2×10^6 cells/mL cell suspension per channel. FITC-GLN, FITC-BSA and BSA-NPs were diluted into serum-free DMEM medium at a final dose of 0.84 mmol/L, 50 μg/mL, and 25 μg/mL, respectively. Cells were exposed to FITC-GLN, FITC-BSA or BSA-NPs in the $\tau = 0.2$ dyne/cm^2 flow condition for 0.5, 1, and 2 h ($n = 3$). For comparison, cells were subjected to the same uptake study under static conditions. The fluorescence images were taken by LSM510 confocal microscopy (Carl Zeiss, Shanghai, China).

2.7. *Immunofluorescence staining*

HK-2 cells cultured under static condition were seeded in confocal culture dishes at a seeding density of 2×10^5/cm^2. Cells cultured under flow condition were as described in Section 2.3. For filamentous actin (F-actin) staining, cells were fixed in 4% paraformaldehyde for 20 min, rinsed three times with PBS, permeabilized with 0.1% Triton X-100 (Sigma−Aldrich) for 10 min, and then rinsed three times with PBS. Next, cells were blocked with 1% BSA at room temperature and incubated with 1:20 diluted TRITC-phalloidin (Invitrogen) at 37 °C for 30 min. Then, the cells were rinsed three times with PBS and stained with 4′,6-diamidino-2-phenylindole (DAPI) (Beyotime Biotechnology, Chengdu, China) for 10 min. The fluorescence images were taken by confocal microscopy.

For immunofluorescence staining of megalin and clathrin, cells were fixed as described above and incubated in 1% BSA at room temperature for 1 h. After rinsing with PBS three times, primary antibodies for megalin or clathrin (rabbit polyclonal IgG, Abcam) were added and incubated at 4 °C overnight. Next, the secondary antibody (goat anti-rabbit IgG/Alexa fluor 488 or FITC, Zhongshanjinqiao Biotechnology, Beijing, China) was added and incubated at room temperature for 1 h. The fluorescence images were taken by confocal microscopy.

2.8. *The in vivo distribution profiles of FITC-BSA-NPs in mice with acute kidney injury*

Before initiation of the acute kidney injury (AKI), all mice were deprived of water but had access to food for 15 h. At the end of the

water restriction, 10 mL/kg of 50% glycerol was administrated into each hind limb of mice intramuscularly as previously reported[25]. All mice were then given free access to water and food. About 2, 12, and 24 h after AKI initiation, mice in all groups were euthanized and blood samples were collected and centrifuged at 2000×*g* (RJ-TDL-40B centrifuge, RUIJIANG instrument) for 15 min at 4 °C to collect plasma samples, which were then subjected to analysis by the Automatic biochemical analyzer for blood creatinine (Cr) and blood urea nitrogen (BUN) levels.

After confirmation of AKI model, both AKI mice and normal mice were administered *via* tail vein injection with FITC-BSA-NPs at an equivalent FITC dose of 1.122 μg/kg and 5 min after administration, mice were sacrificed and their kidneys were collected, and subjected to *ex vivo* imaging (IVIS Spectrum, PerkinElmer, USA).

Next, the isolated kidneys were fixed in 4% paraformaldehyde for 24 h and subjected to gradient dehydration with 10%, 20%, and 30% sucrose solution, respectively. The dehydrated kidneys were embedded with optimal cutting temperature (OCT) embedding agent. A 10 μm frozen section was then cut on a cryostat. The frozen sections were allowed to stand at room temperature for 30 min, and then fixed with ice-cold acetone at 4 °C for 10 min, then washed three times with PBS, and 3% BSA was blocked at room temperature for 30 min. Then, the primary antibody (rabbit polyclonal megalin antibody, dilution 1:1200, Abcam) was incubated in a wet box at 4 °C overnight, and the secondary antibody (Alexa Fluro 647, dilution 1:1000, Abcam) was incubated at room temperature for 50 min in dark, followed by DAPI counterstaining for 10 min. Images were taken on a confocal microscope (Carl Zeiss, Germany).

2.9. *Immunohistochemistry*

Collected kidney tissues were fixed in 4% paraformaldehyde and embedded in paraffin prior to sectioning (4 μm thickness). The sections were dewaxed with a gradient ethanol solution, and then antigen-repaired with 0.01 mol/L citrate buffer solution, and blocked with 3% hydrogen peroxide for 15 min. The primary antibody was then incubated in a wet box at 4 °C overnight, and the secondary antibody was incubated at room temperature for 50 min in the dark. Then use diaminobenzidine (DAB; Dako, Produktionsvej, Denmark) to develop color and control the color development time under the microscope, and hematoxylin was used to counterstain nuclei. Megalin was expressed in the cytoplasm, the cytoplasm of positive cells was stained brown, while the nucleus was stained light blue. To perform semiquantitative analysis, 10 visual fields were randomly selected for each glass slide to be photographed. Next, ImageJ (NIH, Bethesda, MD, USA) was used to analyze and process the positive signals in the selected visual fields. The mean gray value (MOD) of positive staining in the visual field of each slide was calculated respectively. MOD is equal to the integral optical density value (IOD) divided by the measured area. IOD is the optical density value multiplied by the positive area within the measured area.

2.10. *Statistics*

All data were presented as mean ± standard deviation (SD). Statistical analysis was performed using GraphPad Prism 6.0 (GraphPad Software, La Jolla, CA, USA). Semi-quantitative analysis of fluorescence intensity was determined by ImageJ. The means of cell spreading area, uptake efficiency and level of megalin and clathrin expression among groups were compared using Student's *t*-test. *P*-values < 0.05 were considered statistically different.

3. Results

3.1. *Cellular morphology in flow and static conditions*

After attachment, HK-2 cells displayed the typical cobble stone like morphology under static conditions (Fig. 2A). In comparison, cells cultured under the flow condition for 2.5 h displayed the following morphological changes: (i) cells were arranged along the flow field (Fig. 2A); (ii) nuclei and actin filaments became elongated (Fig. 2A); and (iii) the average cell spreading area decreased compared to cells under static conditions ($P < 0.001$) (Fig. 2B).

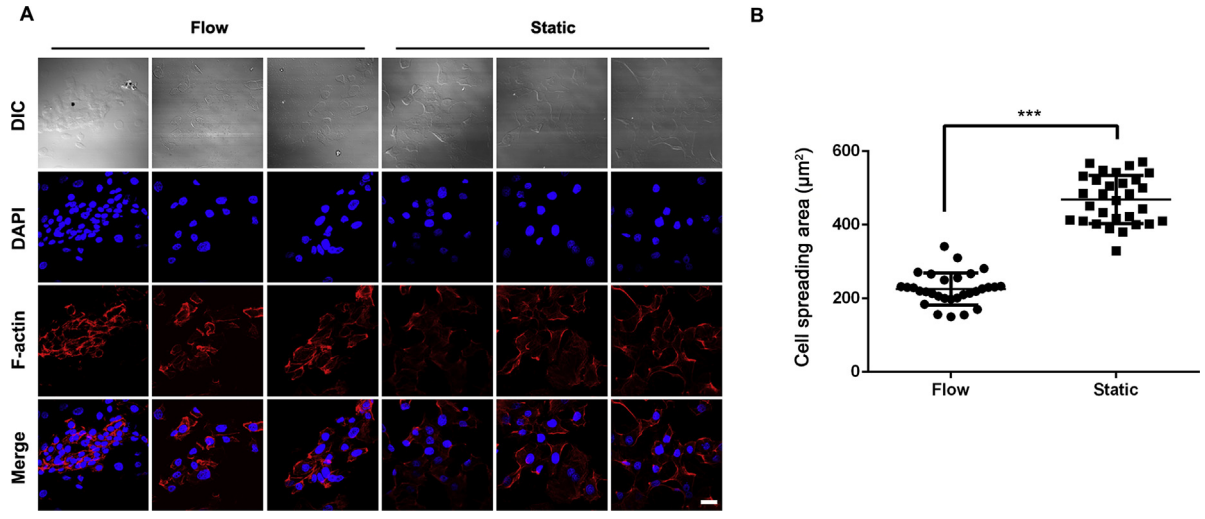

Figure 2 HK-2 morphology under flow and static culture conditions. (A) Fluorescence images of cytoskeleton staining. Cytoskeleton: F-actin (red). Nuclei: DAPI (blue). Scale bar represents 20 μm. (B) Average cell spreading area normalized per cell. The cell spreading area in flow condition is significantly smaller than cells incubated under static conditions ($^{***}P < 0.001$ *vs.* flow).

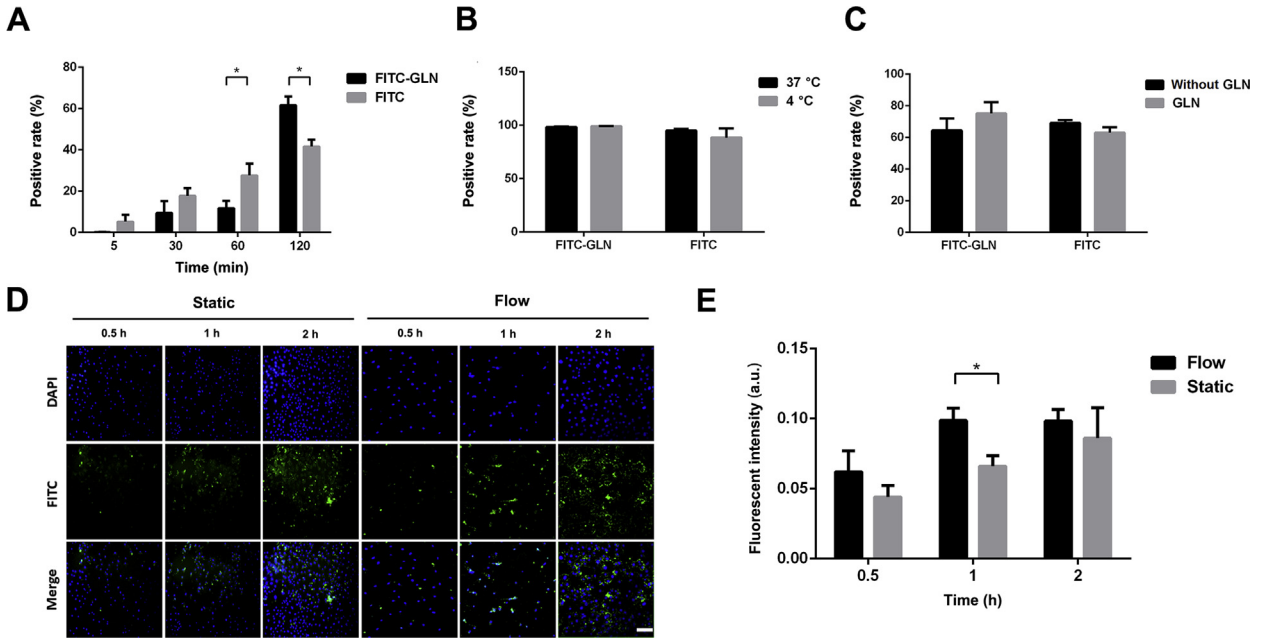

Figure 3 Cellular uptake efficiency of FITC and FITC-GLN in HK-2 cells. (A) Cell uptake at different time points. The uptake of FITC-GLN was lower than that of FITC at 1 h, and the uptake of FITC-GLN was higher than that of FITC at 2 h ($^{*}P < 0.05$ *vs.* FITC). (B) Cell uptake at different temperatures. (C) Cell uptake in the presence of free GLN. (D) Confocal microscopic images of cell uptake in flow and static condition. FITC-GLN, FITC (green); nuclei, DAPI (blue). Scale bar represents 100 μm. (E) Semi-quantitative analysis of fluorescence intensity of FITC-GLN ($^{*}P < 0.05$ *vs.* flow). Data represent mean ± SD ($n = 3$).

3.2. *FITC-GLN cellular uptake in HK-2 cells*

The cellular uptake of FITC and FITC-GLN showed a significant time-dependent manner ($P < 0.001$) and kept increasing over time till reaching a plateau around 2 h. FITC showed higher uptake efficiencies within 60 min, whereas FITC-GLN showed much higher uptake efficiency at 2 h point (Fig. 3A). Meanwhile, the cellular uptake at 4 °C did not show a statistically significant difference compared to the result at 37 °C ($P > 0.05$, Fig. 3B), indicating that the internalization of FITC and FITC-GLN was not energy dependent. Both FITC and FITC-GLN were water soluble small molecules, which may be internalized *via* diffusion driven process. In addition, no significant differences in uptake efficiency were observed between FITC and FITC-GLN in the presence of free glucosamine, and the competitive inhibitor of megalin ($P > 0.05$, Fig. 3C), which further indicates the internalization process is not energy dependent.

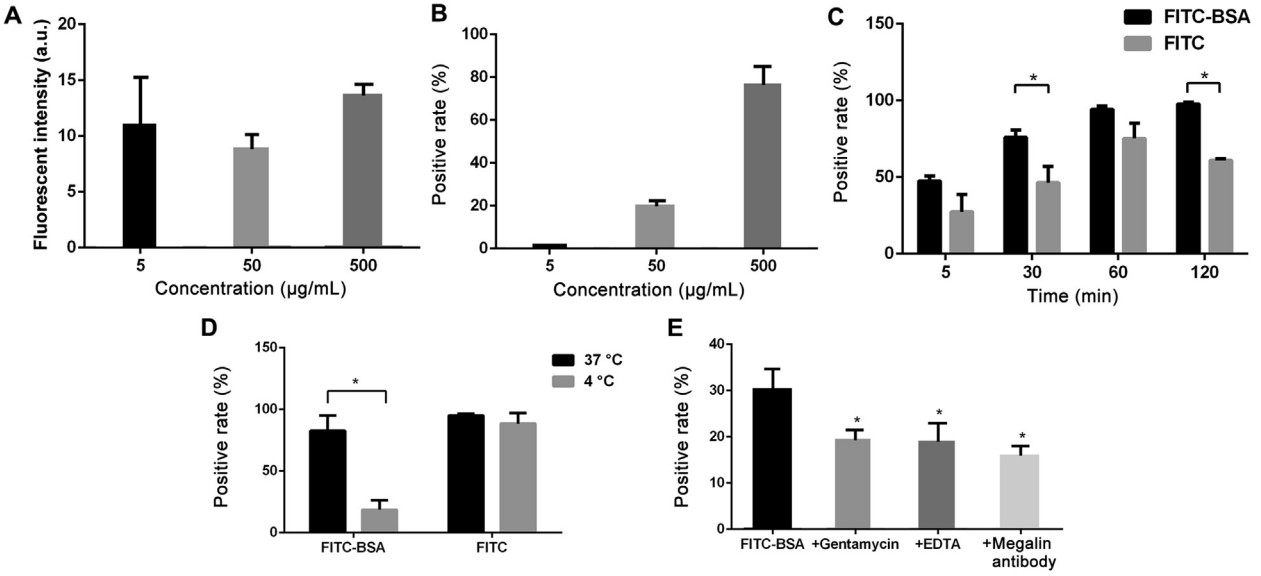

Figure 4 Cell uptake in HK-2 cells by flow cytometry analysis. (A) Cell uptake efficiency at different concentrations of FITC-BSA. (B) The positive rates of FITC-BSA uptake at different concentrations. (C) The positive rates of FITC and FITC-BSA internalization at different time points. (D) Cell uptake at different temperatures. (E) Cell uptake in the presence of megalin inhibitors. $^{*}P < 0.05$ *vs.* FTIC-BSA. Data represent mean ± SD ($n = 3$).

As shown in Fig. 3D, confocal microscopic images showed consistent cell uptake behaviors as observed in flow cytometry analysis. According to semi-quantitative analysis, the cellular uptake of FITC-GLN showed time-dependent increase in both flow and static conditions ($P < 0.001$) (Fig. 3E). The uptake efficiency in flow condition was higher than that in static condition at each time point with a statistically significant difference at 1 h ($P < 0.05$) (Fig. 3D and E).

3.3. *Internalization of FITC-BSA in HK-2 cells under static condition*

According to the flow cytometry analysis, the cell uptake of FITC-BSA in HK-2 cells showed no significant differences across concentrations ranging from 5 to 500 μg/mL ($P > 0.05$, Fig. 4A). The positive rates of HK-2 cells following 2 h FITC-BSA incubation increased significantly with increasing concentrations ($P < 0.05$, Fig. 4B). Both FITC and FITC-BSA showed time-dependent increases in the uptake efficiency that increased over time till reaching a plateau at 1 h. The uptake of FITC-BSA was higher than that of FITC at each given time point and the differences at 30 min and 2 h showed significant higher uptake efficiencies of FITC-BSA than FITC ($P < 0.05$, Fig. 4C). The cell uptake efficiency of FITC-BSA at 37 °C was significantly higher than that at 4 °C ($P < 0.05$), while temperature did not impact the uptake efficiency of FITC (Fig. 4D). In the presence of megalin antibody, gentamycin and EDTA, the cell uptake efficiencies were significantly lower than control ($P < 0.05$, Fig. 4E), which indicated the internalization of FITC-BSA in HK-2 might be an energy-driven process partly mediated by megalin receptors (Fig. 4E).

3.4. *Upregulated levels of megalin in HK-2 cells under flow conditions*

To characterize megalin in HK-2 cells under different culture conditions, we performed immunofluorescence staining of megalin protein. Besides, the differences in cell morphology and cell spreading area, the levels of megalin proteins showed drastic differences between flow and static conditions (Fig. 5A) with a higher fluorescence intensity observed in flow conditions. Semi-quantitative analysis also demonstrated a significantly higher level of megalin in flow conditions than in static conditions ($P < 0.05$, Fig. 5B).

3.5. *Upregulated uptake efficiency of FITC-BSA in HK-2 under flow conditions*

Since an upregulated level of megalin was observed in HK-2 cells under flow conditions, we would like to explore whether this may further impact the uptake efficiency of FITC-BSA in HK-2 cells under flow conditions. As shown in Fig. 6A, the uptake of FITC-BSA in HK-2 cells appeared to increase over time under both flow and static conditions. Meanwhile, the cell uptake efficiency of FITC-BSA in flow conditions was significantly higher than that in static conditions at 1 and 2 h time points ($P < 0.05$, Fig. 6B).

3.6. *Internalization of BSA-NPs in HK-2 cells under static condition*

To explore the internalization behavior of nanoparticles under flow and static conditions, we selected BSA-NPs with average size distributions of 100, 150, and 200 nm. For all three nanoparticles under investigation, their uptake efficiencies showed time-dependent increases from 5 min to 2 h (Fig. 7A). At each given time point, the uptake efficiency of BSA-NPs among groups of different sizes did not show significant differences, indicating a lack of size impact. Next, the mechanistic study of BSA-NPs internalization pathways in HK-2 cells showed that the cell uptake was significantly inhibited at 4 °C and in the presence of sodium azide, indicating that the internalization of BSA-NPs was energy driven. Moreover, groups pre-incubated with chlorpromazine and 5-(*N*,*N*-dimethyl)-amiloride hydrochloride showed significantly lower cell uptake efficiency than the control ($P < 0.01$, Fig. 7B), which suggests that the internalization of BSA-NPs in HK-2 cells occurs mainly through clathrin- and macropinocytosis-mediated endocytosis.

3.7. *Upregulated levels of clathrin heavy chain expression under flow conditions*

Although HK-2 cells demonstrated the expression of clathrin under both flow and static conditions, in flow conditions significantly higher clathrin fluorescence intensity was observed than cells in static conditions ($P < 0.05$, Supporting Information Fig. S5).

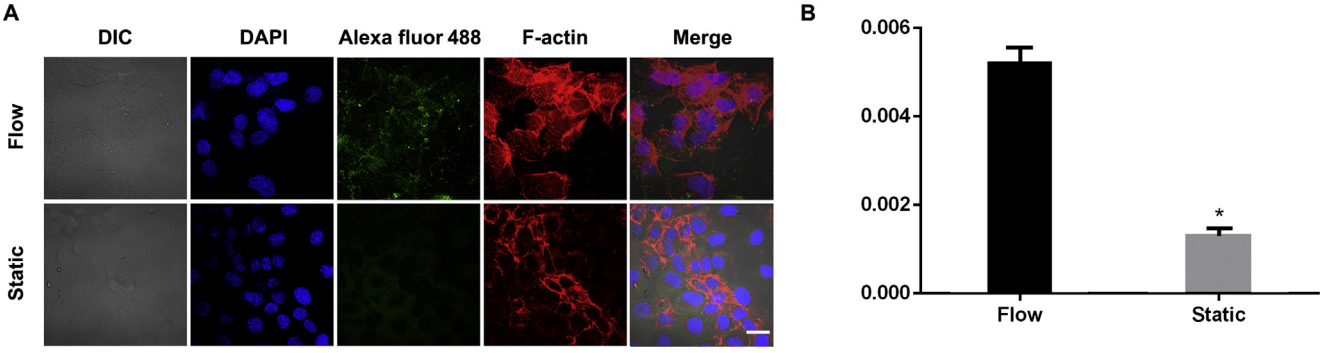

Figure 5 Immunofluorescence staining. Confocal images of HK-2 cells cultured under flow and static conditions (A). Megalin, Alexa fluor 488 (green); cytoskeleton, F-actin (red); nuclei, DAPI (blue). Scale bar represents 10 μm. Semi-quantitative analysis of megalin fluorescence normalized per cell (B). $^{*}P < 0.05$ *vs.* flow. Data represent mean ± SD ($n = 3$).

3.8. *Cell uptake of BSA-NPs in HK-2 cells in flow and static conditions*

Quantitative analysis of fluorescence intensity showed that the cellular uptake of BSA-NPs was time-dependent in both flow and static condition. The cellular uptake efficiency in flow condition was higher than that in static condition with a statistically significant difference at 1 and 2 h ($P < 0.05$), respectively (Fig. 8).

3.9. *The in vivo distribution profiles of FITC-BSA-NPs in AKI mice*

It has been reported that acute renal injury induced by intramuscular injection of glycerin can significantly reduce renal blood flow[26]. To further investigate the effects of changes in fluid shear stress (FSS) *in vivo*, an AKI model was established. Compared with the healthy group, the degree of renal injury following glycerol injection was time-dependent, and the creatinine and urea nitrogen levels reached the peak at 24 h post glycerol injection (Fig. 9A and B). According to the morphological study of renal tissues, a large number of renal tubular epithelial cells were stained and condensed, which became necrotic, disintegrated, and irregularly detached (Fig. 9C). Moreover, a large number of protein casts appeared in the lumen, and the interstitial was observed with capillary congestion with infiltrating inflammatory cells, and some tubular collapse and occlusion (Fig. 9C).

After establishing an acute kidney injury model with reduced renal blood flow, we investigated the distribution of FITC-BSA nanoparticles in the body, and focused on the distribution of nanoparticles in the kidney. *Ex vivo* imaging showed that nanoparticles were mainly distributed in the liver and kidney (Fig. 10C), and the distribution of FITC-BSA nanoparticles in the damaged kidney was significantly reduced compared with the normal kidney (Fig. 10A and B), which was consistent with the

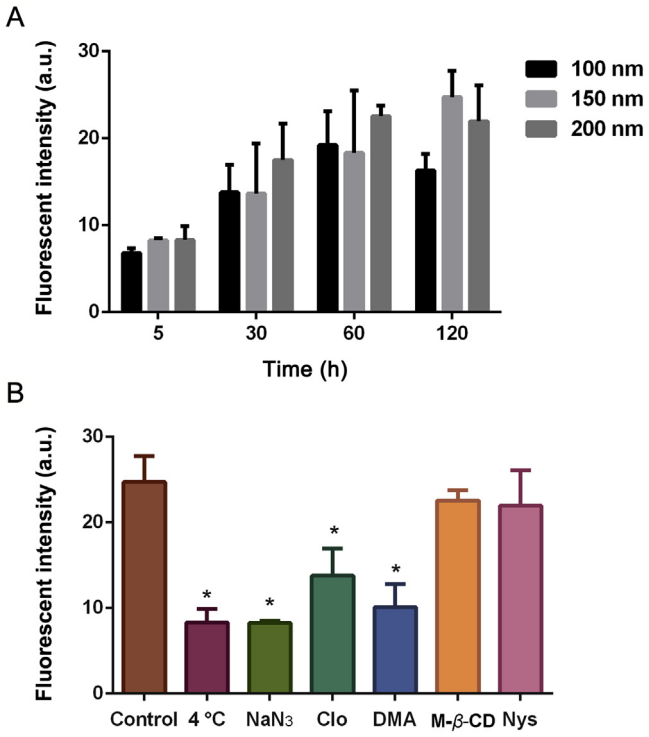

Figure 7 Dynamic and mechanistic study of BSA-NPs internalization pathway in HK-2 cells. Cell uptake of BSA-NPs with three different average sizes (A). Internalization of BSA-NPs in HK-2 cells at 4 °C, pretreated with sodium azide (NaN_3), chlorpromazine (Clo), 5-(*N*,*N*-dimethyl)-amiloride hydrochloride (DMA), methyl-β-cyclodextrin (M-β-CD) and nystatin (Nys), respectively (B). $^{*}P < 0.05$ *vs.* control. Data represent mean ± SD ($n = 3$).

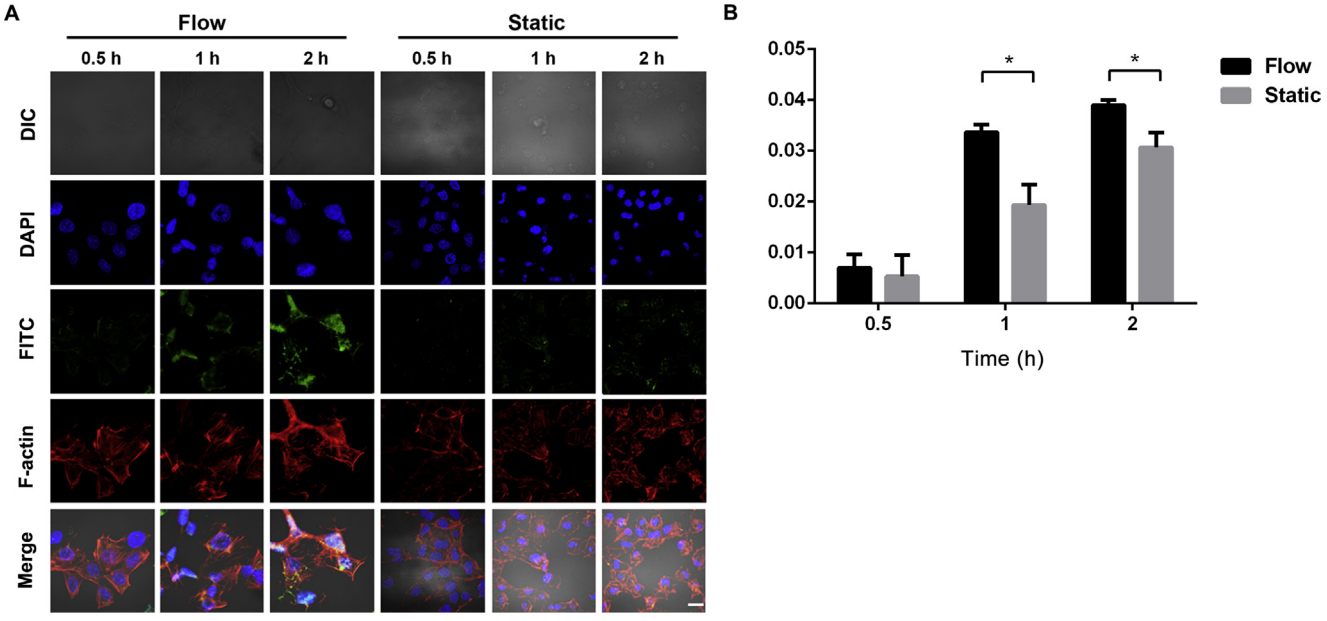

Figure 6 Cell uptake of FITC-BSA in flow and static conditions. Confocal images of FITC-BSA internalization cultured in flow and static conditions (A). FITC-BSA, FITC (green); cytoskeleton, F-actin (red); nuclei, DAPI (blue). Scale bar represents 10 μm. Semi-quantitative analysis of FITC-BSA fluorescence intensity normalized per cell (B). $^{*}P < 0.05$. Data represent mean ± SD ($n = 3$).

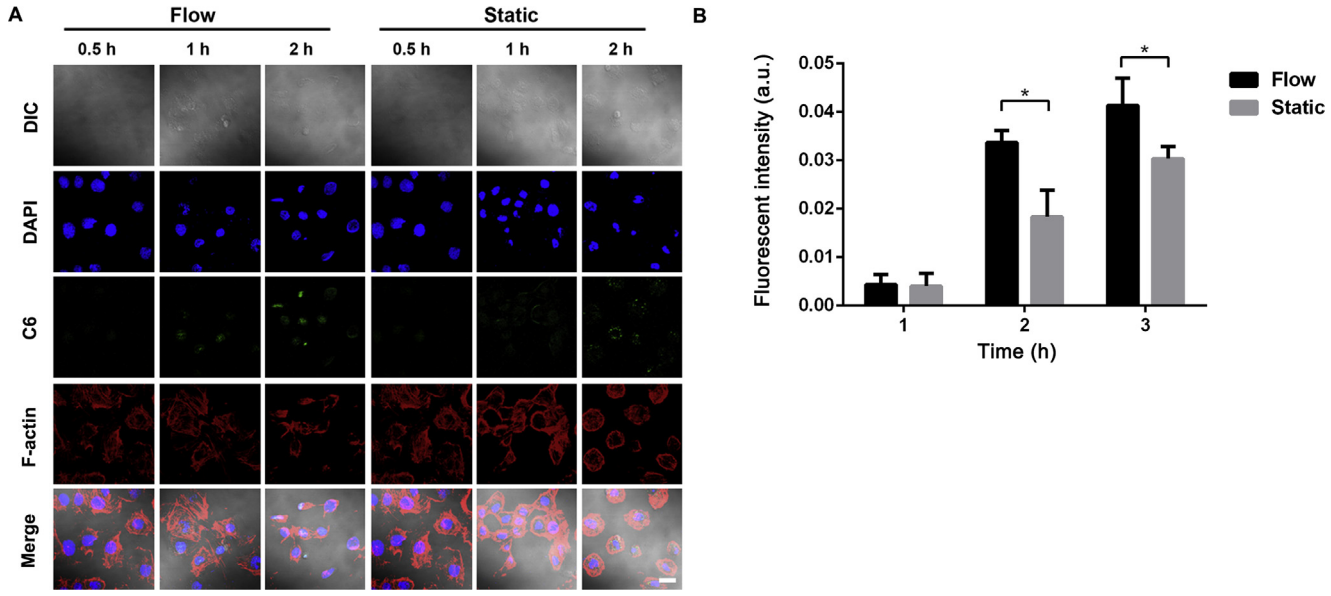

Figure 8 Cellular uptake of BSA-NPs in flow and static conditions. Confocal images of BSA-NPs uptake in flow and static conditions (A). BSA-NPs, C6 (green); cytoskeleton, F-actin (red); nuclei, DAPI (blue). Scale bar represents 10 μm. Semi-quantitative analysis of fluorescence intensity of BSA-NPs uptake as normalized per cell (B). $^{*}P < 0.05$ *vs.* flow. Data represent mean ± SD ($n = 3$).

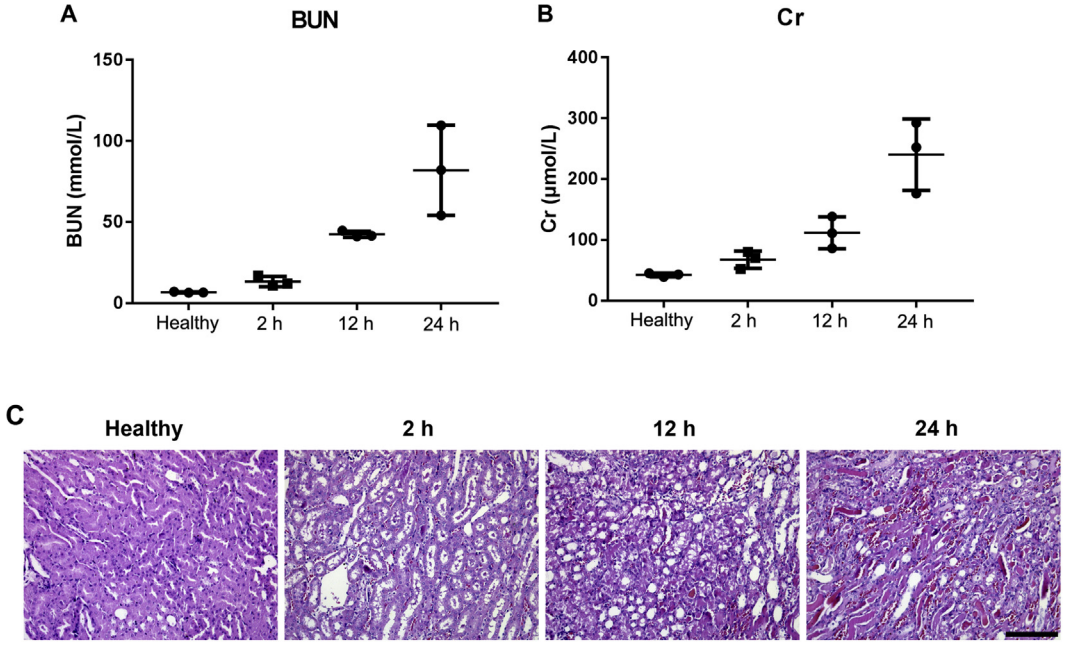

Figure 9 Analysis of blood urea nitrogen (BUN) (A) and serum creatinine (Cr) (B) levels of AKI mice after model initiation. Data represent mean ± SD ($n = 3$). Representative images of H&E stained kidney sections of healthy and AKI mice at different time periods post model initiation (C). Scale bar represents 200 μm.

results *in vitro*, suggesting that the decrease in renal blood flow may reduce the expression of Megalin receptor, thereby reducing the uptake of nanoparticles in the kidney (Fig. 10).

Next, the colocalization analysis of the distribution of FITC-BSA nanoparticles in the kidney and the expression of megalin by immunofluorescence staining with frozen sections was performed. Confocal microscopic analysis showed that the distribution of nanoparticles overlapped with the distribution of megalin, suggesting that the renal uptake of nanoparticles was mainly driven by megalin-mediated internalization. Additionally, FITC-BSA nanoparticles were mainly distributed in the renal tubules (Fig. 11A). The expression patterns of megalin in renal tissues were further quantitatively analyzed by immunohistochemistry. The semi-quantitative analysis showed that AKI induced renal

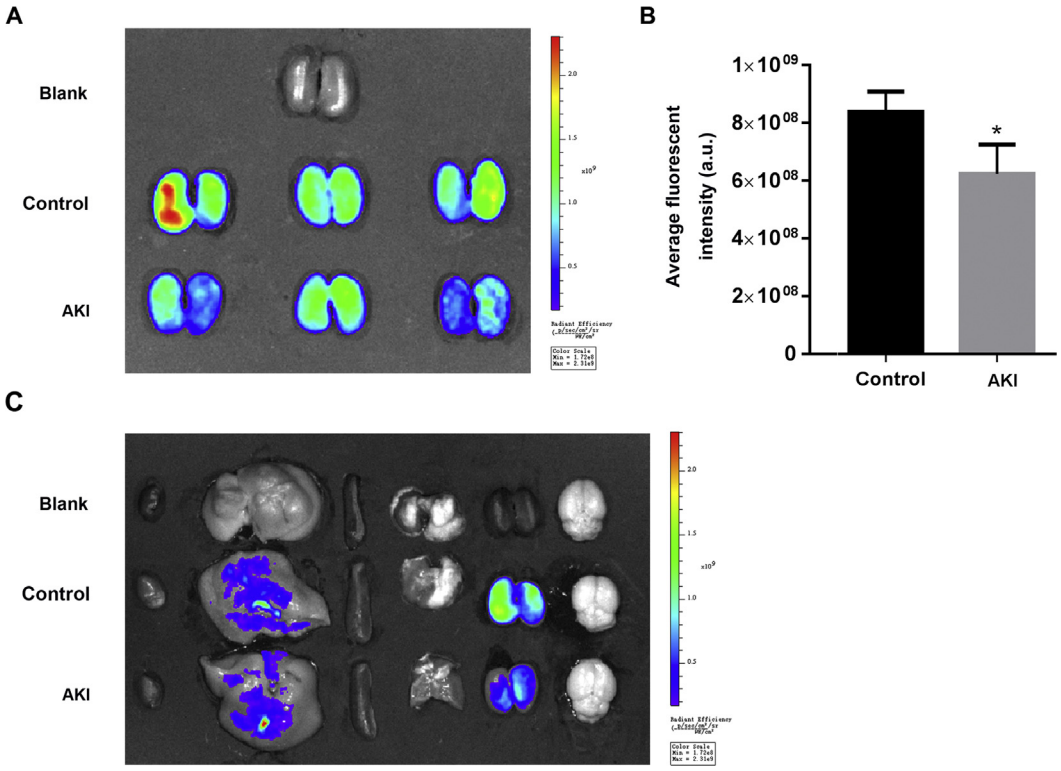

Figure 10 *In vivo* distribution. Representative *ex vivo* fluorescence image of kidneys (A) and the semiquantitative analysis of fluorescence intensity of kidneys (B). Representative *ex vivo* fluorescence image of major organs from mice sacrificed 5 min post i.v. injection of FITC-BSA-NPs (C). Data represent as mean ± SD ($n = 3$), *$P<0.05$ *vs*. Control.

injury led to reduced levels of megalin expression (Fig. 11B), which suggests that the renal injury likely result in decreased renal blood flow, thereby down-regulating the levels of megalin in the renal tubules.

4. Discussion

As compared to cells under static conditions, cells cultured under flow conditions displayed elongated nuclei and actin filaments with decreased cell spreading area. According to previous publications, flow-dependent mechanism in proximal tubule cells was that FSS created binding moment on microvilli at insertion into actin cytoskeleton[27]. For example, in response to FSS in culture, cells may reorganize their actin and junctional proteins, including the disseminations of basal actin stress fibers, formation of adherens and tight junction, and accumulation of focal adhesion proteins in the basement membrane. Thus, future studies may focus on the membrane proteins associated with either the apical or the basolateral side to elucidate how HK-2 cells respond to FSS.

In our study, FITC-GLN did not show significantly higher internalization efficiency in HK-2 as compared to FITC only. Also, mechanistic studies revealed that the internalization of FITC-GLN into HK-2 cells was mainly diffusion driven, similar to the uptake of free FITC. Although cellular uptake of FITC-GLN in flow conditions was higher than under static conditions during the study period, no significant differences were observed between the two conditions ($P > 0.05$) by the end of the study. This might be due to the fact that flow conditions caused the extracellular drug concentration to drop slowly, which maintained the concentration difference between intracellular and extracellular at a higher level. However, as long as the concentration difference reached the gradient to maintain free diffusion, the uptake efficiency remained near constant. Previous findings indicated that GLN derived conjugate systems may be internalized *via* specific interaction with megalin receptors[14]. From our observation, the presence of GLN in FTIC-GLN did not change the internalization behavior of FITC into HK-2 cells, which is likely due to the loss of free 2-amino group in GLN when forming a covalent bond with FITC. The presence of free 2-amino group in GLN has proven to be a critical functional group for the recognition of megalin receptors[28]. Thus, it would be interesting to see how FSS may impact the internalization behavior of a 2-glucosamin conjugated system with a free 2-amino group.

To further explore the impact of FSS on receptor-mediated endocytosis, BSA was selected as the model carrier due to its specific interaction with the megalin-cubilin proteins during reabsorption[29,30]. For FITC-BSA, a rapid and sustained upregulation in uptake efficiency was observed in HK-2 cells upon exposure to physiologically relevant levels of FSS[4]. Our study further suggests that the internalization of BSA in HK-2 might be an energy-driven process partly mediated by megalin receptors. Under flow conditions, the upregulated levels of megalin receptor expression may contribute to the augmented uptake efficiency of FITC-BSA in HK-2, consistent with report from the literature[4]. Therefore, we infer that albumin may enter HK-2 cell *via* megalin receptor-mediated endocytosis and applying FSS may promote cell uptake of albumin by upregulating the expression of megalin receptors. However, the underlying mechanisms require further

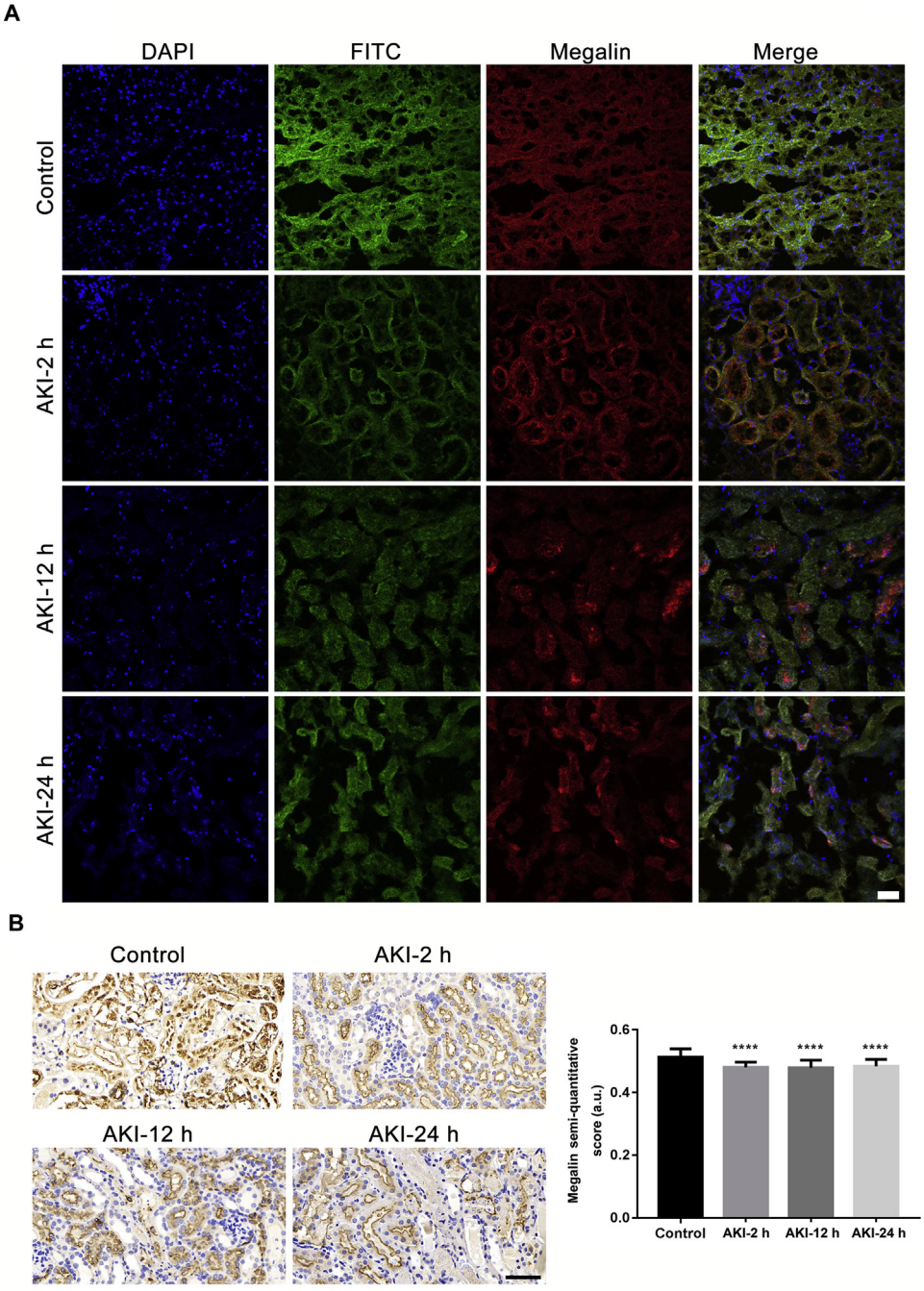

Figure 11 Megalin colocalization *via* confocal microscopy (A) and the expression of megalin in renal tissue of mice in AKI 2, 12, 24 h, and healthy groups (B, IHC×, I). Confocal images of megalin colocalization analysis of FITC-BSA-NPs in renal tissue. FITC-BSA-NPs (green); megalin, Alexa Fluro 647 (red); nuclei, DAPI (blue), scale bar represents 100 μm. Immunohistochemical images, scale bar represents 50 μm. Data represent mean ± SD ($n = 3$). $^{****}P < 0.0001$ *vs.* Control.

investigation, which might involve increased intracellular Ca^{2+} concentrations and purinergic signaling in response to FSS-dependent ciliary bending that triggered an increase in apical endocytosis[4].

Next, our study looked into the effect of FSS on the internalization of BSA-NPs in HK-2 cells. Gomez-Garcia et al.[31] performed a study on the nanoparticle localization in blood vessels, which showed that nanoparticle accumulation in endothelial cells *in vitro* was affected by shear stress and flow pattern. FSS-stimulated apical endocytosis in proximal tubule was previously found to be initiated *via* a clathrin- and dynamin-dependent pathway[4]. In our study of BSA-NPs internalization pathways in HK-2 cells, the uptake of BSA-NPs was found to be mediated by clathrin-mediated and micropinocytosis pathways. Combined with

the immunofluorescence staining results of clathrin, FSS appeared to upregulate the expression level of clathrin in HK-2 cells and lead to a higher uptake efficiency of BSA-NPs in flow conditions. The *in vivo* distribution profiles of BSA-NPs in kidney tissue also showed that albumin nanoparticles could achieve kidney targeted drug delivery and enter renal tubules (Supporting Information Fig. S6), demonstrating the great potential of using albumin nanoparticles as an efficient delivery system for targeted therapies of renal diseases.

5. Conclusions

A microfluidic system has been established to elucidate the internalization behavior of kidney-targeted drug delivery systems under flow conditions. Our findings suggest that FSS had no impact on the diffusion driven internalization pathway, whereas it impacted the energy driven internalization of macromolecular carriers such as BSA and albumin nanoparticles by altering the morphology and the receptor expression pattern of RTECs. Such findings may provide useful insights in the development and evaluation of kidney-targeted drug delivery systems.

Acknowledgments

The authors are grateful for the financial support from the National Natural Science Foundation of China (81773654 and 81503018), National Key Research and Development Plan of China (2017YFC1104601), Sichuan University Fund for Excellent Young Scholars (2017SCU04A23, China) and Sichuan Youth Science and Technology Innovation Research Team Funding (2016TD0001, China).

Author contributions

Yao Fu conceived and planned the study, revised the manuscript. Yingying Xu and Shuo Qin carried out the experiments, generated and analyzed data, and drafted the original manuscript. Yining Niu helped with animal studies. Tao Gong and Zhirong Zhang participated in data analysis.

Conflicts of interest

The authors declare no conflicts of interests.

Appendix A. Supporting information

Supporting data to this article can be found online at https://doi.org/10.1016/j.apsb.2019.11.012.

References

1. Khan KN, Hard GC, Alden CL. Kidney. In: Haschek WM, Rousseaux CG, Wallig MA, editors. *Haschek and Rousseaux's handbook of toxicologic pathology*. 3rd ed. Utah: Academic Press; 2013. p. 1667−773.
2. Lawrence EA, Doherty D, Dhanda R. Function of the nephron and the formation of urine. *Anaesth Intensive Care* 2018;**19**:249−53.
3. Duan Y, Weinstein AM, Weinbaum S, Wang T. Shear stress-induced changes of membrane transporter localization and expression in mouse proximal tubule cells. *Proc Natl Acad Sci U S A* 2010;**107**:21860−5.
4. Raghavan V, Rbaibi Y, Pastor-Soler NM, Carattino MD, Weisz OA. Shear stress-dependent regulation of apical endocytosis in renal proximal tubule cells mediated by primary cilia. *Proc Natl Acad Sci U S A* 2014;**111**:8506−11.
5. Ross TD, Coon BG, Yun S, Baeyens N, Tanaka K, Ouyang M, et al. Integrins in mechanotransduction. *Curr Opin Cell Biol* 2013;**25**:613−8.
6. Dimmeler S, Assmus B, Hermann C, Haendeler J, Zeiher AM. Fluid shear stress stimulates phosphorylation of Akt in human endothelial cells-involvement in suppression of apoptosis. *Circ Res* 1998;**83**:334−41.
7. Wang Y, Gong T, Zhang ZR, Fu Y. Matrix stiffness differentially regulates cellular uptake behavior of nanoparticles in two breast cancer cell lines. *ACS Appl Mater Interfaces* 2017;**9**:25915−28.
8. Liu CP, Hu Y, Lin JC, Fu HL, Lim LY, Yuan ZX. Targeting strategies for drug delivery to the kidney: from renal glomeruli to tubules. *Med Res Rev* 2018;**257**:169−80.
9. Haase M, Kellum JA, Ronco C. Subclinical AKI—an emerging syndrome with important consequences. *Nat Rev Nephrol* 2012;**8**:735−9.
10. Kellum JA, Bellomo R, Ronco C. Definition and classification of acute kidney injury. *Nephron Clin Pract* 2008;**109**:c182−7.
11. Levey AS, Eckardt KU, Tsukamoto Y, Levin A, Coresh J, Rossert J, et al. Definition and classification of chronic kidney disease: a position statement from Kidney Disease: improving Global Outcomes (KDIGO). *Kidney Int* 2005;**67**:2089−100.
12. Zhou P, Sun X, Zhang Z. Kidney-targeted drug delivery systems. *Acta Pharm Sin B* 2014;**4**:37−42.
13. Stridh S, Palm F, Hansell P. Renal interstitial hyaluronan: functional aspects during normal and pathological conditions. *Am J Physiol Regul Integr Comp Physiol* 2012;**302**:R1235−49.
14. Lin Y, Li Y, Wang X, Gong T, Zhang L, Sun X. Targeted drug delivery to renal proximal tubule epithelial cells mediated by 2-glucosamine. *J Control Release* 2013;**167**:148−56.
15. Zhang Y, Sun T, Jiang C. Biomacromolecules as carriers in drug delivery and tissue engineering. *Acta Pharm Sin B* 2018;**8**:34−50.
16. Yin J, Wang J. Renal drug transporters and their significance in drug−drug interactions. *Acta Pharm Sin B* 2016;**6**:363−73.
17. Elzoghby AO, Samy WM, Elgindy NA. Albumin-based nanoparticles as potential controlled release drug delivery systems. *J Control Release* 2012;**157**:168−82.
18. Li D, Zhang M, Xu F, Chen Y, Chen B, Chang Y, et al. Biomimetic albumin-modified gold nanorods for photothermo-chemotherapy and macrophage polarization modulation. *Acta Pharm Sin B* 2018;**8**:74−84.
19. Byun CK, Abi-Samra K, Cho YK, Takayama S. Pumps for microfluidic cell culture. *Electrophoresis* 2014;**35**:245−57.
20. Jang KJ, Mehr AP, Hamilton GA, McPartlin LA, Chung S, Suh KY, et al. Human kidney proximal tubule-on-a-chip for drug transport and nephrotoxicity assessment. *Integr Biol (Camb)* 2013;**5**:1119−29.
21. Ikemoto K, Sakata I, Sakai T. Collision of millimetre droplets induces DNA and protein transfection into cells. *Sci Rep* 2012;**2**:289.
22. Lomis N, Westfall S, Farahdel L, Malhotra M, Shum-Tim D, Prakash S. Human serum albumin nanoparticles for use in cancer drug delivery: process optimization and *in vitro* characterization. *Nanomaterials (Basel)* 2016;**6**:1−17.
23. Kang T, Park C, Choi JS, Cui JH, Lee BJ. Effects of shear stress on the cellular distribution of polystyrene nanoparticles in a biomimetic microfluidic system. *J Drug Deliv Sci Technol* 2016;**31**:130−6.
24. Langer K, Balthasar S, Vogel V, Dinauer N, von Briesen H, Schubert D. Optimization of the preparation process for human serum albumin (HSA) nanoparticles. *Int J Pharm* 2003;**257**:169−80.
25. Qiao H, Sun M, Su Z, Xie Y, Chen M, Zong L, et al. Kidney-specific drug delivery system for renal fibrosis based on coordination-driven assembly of catechol-derived chitosan. *Biomaterials* 2014;**35**:7157−71.
26. Huang RS, Zhou JJ, Feng YY, Shi M, Guo F, Gou SJ, et al. Pharmacological inhibition of macrophage Toll-like receptor 4/nuclear factor-kappa B alleviates rhabdomyolysis-induced acute kidney injury. *Chin Med J (Engl)* 2017;**130**:2163−9.

27. Weinbaum S, Duan Y, Satlin LM, Wang T, Weinstein AM. Mechanotransduction in the renal tubule. *Am J Physiol Renal Physiol* 2010; **299**:F1220−36.
28. Yuan ZX, Zhang ZR, Zhu D, Sun X, Gong T, Liu J, et al. Specific renal uptake of randomly 50% *N*-acetylated low molecular weight chitosan. *Mol Pharm* 2009;**6**:305−14.
29. Birn H, Christensen EI. Renal albumin absorption in physiology and pathology. *Kidney Int* 2006;**69**:440−9.
30. Yuan ZX, He XK, Wu XJ, Gao Y, Fan M, Song LQ, et al. Peptide fragments of human serum albumin as novel renal targeting carriers. *Int J Pharm* 2014;**460**:196−204.
31. Gomez-Garcia MJ, Doiron AL, Steele RRM, Labouta HI, Vafadar B, Shepherd RD, et al. Nanoparticle localization in blood vessels: dependence on fluid shear stress, flow disturbances, and flow-induced changes in endothelial physiology. *Nanoscale* 2018; **10**:15249−61.